Role of Noise in Spontaneous Activity of Networks of Neurons on Patterned Silicon Emulated by Noise–activated CMOS Neural Nanoelectronic Circuits

NANO EXPRESS

PAPER

Role of Noise in Spontaneous Activity of Networks of Neurons on Patterned Silicon Emulated by Noise–activated CMOS Neural Nanoelectronic Circuits

Ramin Hasani[1,2,3], **Giorgio Ferrari**[1], **Hideaki Yamamoto**[4], **Takashi Tanii**[5] and **Enrico Prati**[6]

[1] Dipartimento di Elettronica, Informazione e Bioingegneria, Politecnico di Milano, Via Colombo 81, I–20133 Milano, Italy
[2] Department of Computer Engineering, Technische Universität Wien, Treitlstrasse 3-3, 1040, Vienna, Austria
[3] Computer Science and Artificial Intelligence Lab (CSAIL), Massachusetts Institute of Technology (MIT), 32 Vassar St., Cambridge, MA, United States of America
[4] Research Institute of Electrical Communication, Tohoku University, 2-1-1 Katahira, Aoba-ku, Sendai 980-8577, Japan
[5] School of Science and Engineering, Waseda University, 3-4-1 Ohkubo, Shinjuku, Tokyo 169-8555, Japan
[6] Istituto di Fotonica e Nanotecnologie, Consiglio Nazionale delle Ricerche, Piazza Leonardo da Vinci 32, I–20133 Milano, Italy

E-mail: enrico.prati@cnr.it

OPEN ACCESS

RECEIVED
31 December 2020

REVISED
14 March 2021

ACCEPTED FOR PUBLICATION
26 March 2021

PUBLISHED
14 June 2021

Keywords: patterned adhering scaffolds, cortical microcircuits, tonic spiking, silicon brains, neuromorphic engineering, noise assisted information processing

Supplementary material for this article is available online

Abstract

Background noise in biological cortical microcircuits constitutes a powerful resource to assess their computational tasks, including, for instance, the synchronization of spiking activity, the enhancement of the speed of information transmission, and the minimization of the corruption of signals. We explore the correlation of spontaneous firing activity of ≈ 100 biological neurons adhering to engineered scaffolds by governing the number of functionalized patterned connection pathways among groups of neurons. We then emulate the biological system by a series of noise-activated silicon neural network simulations. We show that by suitably tuning both the amplitude of noise and the number of synapses between the silicon neurons, the same controlled correlation of the biological population is achieved. Our results extend to a realistic silicon nanoelectronics neuron design using noise injection to be exploited in artificial spiking neural networks such as liquid state machines and recurrent neural networks for stochastic computation.

1. Introduction

The correlation of biological and noise-solicited CMOS artificial spiking neurons between small distinct populations of neurons is modulated and compared by controlling the number of inter-connected neurons and synapses. The exploration of neuronal microcircuits [1–10] as the building blocks of the complex behavioral motifs is not only supported by experimental evidence [11–15] but also substantiated by mathematical models [16–18].

The study of biological neural circuits stands as an intermediate step towards comprehending and controlling the building blocks of efficiently engineered artificial neural networks [19–22]. These neural circuits function in the presence of measurable background noise and studies showed that this stochastic environment acts as a resource for enhancing neural computations [23–31]. Computational models of neural circuits confirmed these experimental observations [32–37]. Experiments on a randomly-wired network of spiking neurons showed that a considerable amount of knowledge is stored inside the nervous system enabled by this stochastic background noise [38–41].

In this regard, networks of stochastic spiking neurons have been used for solving constraint satisfaction problems where noise is believed to play a key role in the problem-solving ability of the human brain [42–45]. For instance, neurons' activity is correlated in the isolated regions of the auditory cortex to which the neuron

belongs [46, 47]. The correlation among distinct groups of neurons (*islands* for brevity from now on) is directly proportional to the number of interneuron connections and interneuronal correlation. Furthermore, synchronization among neuronal populations in motor cortical regions where they communicate through interneurons may play an important role in cognitive-motor processes [48, 49]. Propagation of spiking activity amongst different neuronal modules has been studied and reviewed in [50–52]. Refinements of a natural communication stimulus are permitted by the correlated neural activity in fish [53]. A mechanism by which neural circuits effectively shape their signal and noise in concert has been demonstrated, enabling the minimization of the corruption of signal by noise and by enhancing the speed of information transmission [54, 55].

Previously, we separately explored the island size-dependence of synchronized activity in living neuronal networks [56], the white noise enhancement of the transmission of spiking activity along a linear chain of artificial neurons based on discrete components, and its inter-spike interval (ISI) by varying the amplitude of the noise [35], and spike-timing-dependent plasticity in CMOS artificial neurons assisted by noise during training [57]. CMOS artificial neurons [57–60] serve as an effective platform to emulate biologically plausible neurons implementing universal functionalities speculated for toy block microcircuits and to build deep models [61].

In the present study we functionalize silicon patches to attach real neurons forming an SNN, and exploit the role of noise [62] in a network of simulated CMOS artificial spiking neurons in order to reverse engineer the features of the SNN of real neurons. Figure 1 graphically represents an overview of our research framework. To observe the change of correlation rate of spiking activity of neurons among different islands of neurons by adding interconnection neurons, we performed experiments with real in-vitro neurons. The spiking activity of four islands of randomly-wired spiking neurons with sufficiently interconnected neurons is investigated. *The correlation of spiking activities drastically rises by increasing the number of pathways between islands where the neurites can grow.* We then exploit a nature-inspired physical disturbance such as noise (by adopting the same ring topology of four-islands of the first part) on CMOS silicon neurons. The elementary blocks, including CMOS neurons, excitatory and inhibitory synapses, are combined to constitute a network of spiking neurons ready to investigate the influence of solicitation by a noise-injector circuit. The noise response of the silicon neuron to both white and pink noise spectra is then thoroughly discussed. The silicon neuron microcircuits are utilized to investigate the correlation of noise-assisted spiking activity of the four-islands topology in analogy with biological neurons. *As a final result, we demonstrate how the correlation of spiking activity among isolated sub-networks ignited by distinct background noise is progressively increased?*We show this by adding interconnection elements between neurons of different sub-networks and more efficiently by adopting multiple synapses, ensuring firing to more input neurons, by achieving the artificial microcircuit counterpart of the biological network results.

2. Methods

In this section, we introduce our methods for studying noise propagation in distinct neuronal regions. First, we discuss the experimental set-up for a group of biological neurons. In the second section, we design a quasi-equivalent setting for the artificial model of the experimental part to perform predictions on the dynamics of the real network.

2.1. Experimental setup for investigating noise propagation in biological neural circuits

Biological neurons, which are obtained from animal brains [63] or stem cell differentiation [64], can be cultivated in-vitro under a defined physicochemical condition. Neurons are adherent cells, and hence an appropriate scaffold is essential for their growth. A number of microfabrication methods, including semiconductor lithography or soft lithography, have been utilized to engineer the scaffold to control the growth area at single-cell or multi-cellular scales [56, 65–68].

After approximately a week in culture, neuronal networks begin to form synaptic connections and spontaneously generate bursting activity that is highly synchronized within the network [29, 56]. We previously showed using micropatterned rat cortical neurons that neuronal correlation in the spontaneous bursting activity decreases with the size of the network [56]. This section uses a similar culture to show that correlation between a group of living neurons can be regulated by altering the number of neurite guidance pathways that bridge neuron islands. The experimental results and their analyses herein are obtained from independent datasets from those presented in a previous publication [69].

The materials and methods used in fabricating micropatterned substrates, culturing primary neurons, and recording spontaneous neural activity have been described previously [56, 68]. Briefly, *poly − D − lysine* and *2 − [methoxy (polyethleneoxy)propyl]trimethoxysilane* were used as cell-permissive and non-permissive layers, respectively, and were patterned on a glass coverslip using electron-beam lithography. The micropatterns used

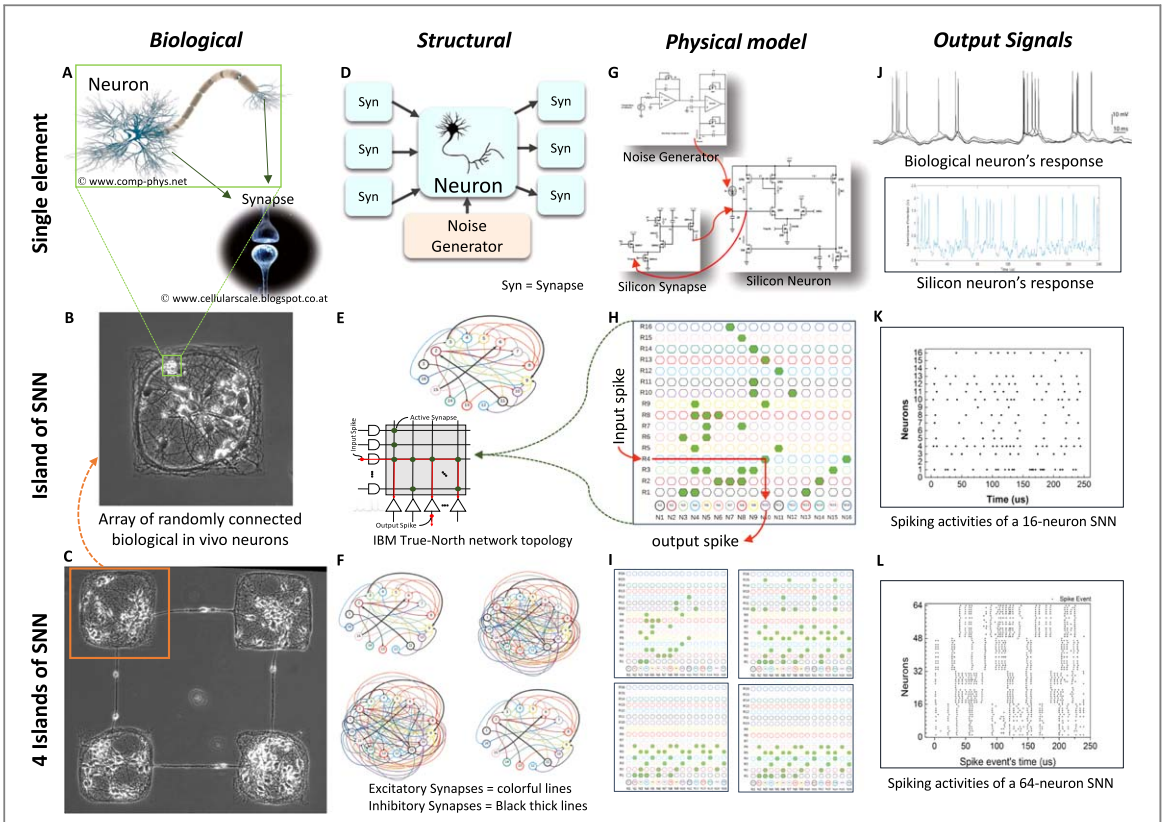

Figure 1. A General framework for modeling and exploiting noise-induced spiking activity from biological to silicon neurons. The fine structure of the neural network elements, including neurons and synapses, together with their neural network structure, is shown in biological, structural, and physical model representation. A) Anatomy of a single neuron with a zoom-in on synapses region (B) A network of in-vitro neurons in a random topology connectome based on the artificial scaffold. (C) Four islands of biological neurons linked to each other by a single pathway for interneurons where we observe the propagation of the correlation of spiking activity of single neurons. (D) Structural representation of a stochastic model of spiking neurons and chemical synapses. (E) Representation of a network of 16 neurons randomly connected. The network design is inspired by the structural topology used by IBM TrueNorth [70]. (F) Structure of four islands of randomly connected CMOS spiking neurons (here shown isolated from each other). We simulate the circuital analogous of the experiment performed on real neurons by CMOS SNNs exposed to white noise. (G) Stochastic model of spiking neuron designed in a 0.35 μm CMOS technology together with the designed CMOS synapses. (H) Network of 16 CMOS neurons and 256 synapses designed in a 0.35 μm CMOS technology. The network is designed such that any arbitrarily many-to-many topology can be implemented. (I) 4 islands of CMOS neurons and synapses. The network consists of 64 neurons and 1024 synapses. (J) output response of a biological and a CMOS neuron to the white noise signal. (K) Raster plot of the spiking activity of single neurons of the network of (H), where a white noise source excites one neuron. (L) Raster plot of the spiking activity of 64 neurons of the network of (I), where neurons of each island are excited by a distinct source of white noise.

in the current experiment consisted of four square islands of 200 $\times$ 200 μm^2 and 5 μm-wide lines that interconnect the island. Three geometries with a different number of interconnecting lines were compared, i.e., no-bond and triple-bond structures, which have zero and three lines between a pair of islands.

Primary neurons were obtained from embryonic rat cortices, plated on the micropatterned coverslips, and cultured for ten days. Then, the cells were loaded with the fluorescence calcium indicator Fluo-4 AM (Molecular Probes), and their spontaneous activity was measured by calcium imaging. Images were obtained every 200*ms* for 6 or 9 min using an inverted microscope (Nikon Eclipse TE300) equipped with a 20 $\times$ objective lens (numerical aperture, 0.75) and a cooled-CCD camera (Hamamatsu Orca-ER). The image sequences were later analyzed offline using the ImageJ (NIH) and custom-written Perl programs [56].

Representative phase-contrast micrographs of living neuronal networks grown on the micropatterned substrate are shown in figures 1(B) and 1(C). Neurons adhered and grew neurites only on the permissive domains. Very little non-specific adhesion or neurite growth was observed in the non-permissive area. The number of cells in each network was counted from the images. It was evaluated to be 148, 143, and 154 cells for the no-bond, single-bond, and triple-bond structures.

Next, spontaneous neural activity was measured by fluorescence calcium imaging, and the effect of changing the number of interconnections between neuronal islands was analyzed by evaluating the Pearson correlation coefficient. The correlation coefficient of neuron pairs is calculated using the Pearson correlation coefficient equation described in appendix B. We discuss our observations thoroughly in the Results section.

2.2. CMOS artificial neural networks setting for quantifying the rate of correlated-activity in distinct neuronal islands

To emulate the noise activation of biological neurons, we first define a biologically plausible silicon neuron model so that response to electronic noise injection is realistic. The neuron is designed based on a simplified Hodgkin-Huxley (HH) spiking neuron model [71], which is designed and simulated in a 0.35 μm CMOS technology [72]. A sodium-potassium conductance-based model of spiking neurons biased in the sub-threshold regime is implemented. Neurons are designed with a lower time-constant to spike three orders of magnitude faster than real neurons (more details on the implementation are provided in appendix A). Such speed-mode implementation allows faster data processing, requires smaller capacitor values, and as a result, reduces the physical size of the circuit. To model a background noise, we designed a voltage to current converter capable of delivering a zero-mean white and pink current noise to the neurons (see appendix A). Typically, noise is naturally present in CMOS devices, ranging from white and pink ($1/f$) noise [73], to telegraph noise [74–76], to $1/f^{1/2}$ noise [77, 78], rooted in the atomistic scale. The most straightforward strategy consists of amplifying such natural noise and exploiting it in the circuit by injection in the selected nodes.

Synapses are junctions where neurons communicate with each other. Chemical synapses can be either excitatory or inhibitory. We adopted a synapse circuit model, called CMOS differential-pair integrator (DPI) [79], to wire neurons.

To emulate and reverse-engineer the experimental system topology constructed from four neuronal islands of biological neurons adhering stick to the patterned region, we designed and simulated a network of spiking neurons comprising 64 silicon neurons and 1024 DPI synapses in the presence of white background noise. Individual islands comprising 16 silicon neurons and 256 synapses are designed and are exposed to white noise. Next, the correlation of spiking activity of the four neuronal islands is controlled by tuning the number of the equivalent of interneurons connecting distinct neuronal islands and the number of synapses excited by the same output interneuron. The observations are quantitatively accounted for by employing a correlation coefficient matrix of stochastic events (Appendix B for methods). Figure 3(A) represents a network of 16 silicon neurons and 256 reconfigurable synapses. To be consistent with networks of typical hybrid systems of real neurons on artificial solid-state structures, we adopted a ratio between inhibitory and excitatory synapses in the range 5% to 10%. In our case, such a ratio is set to 8%. The output of each neuron is connected to 16 synapses presented in a row in order to be able to connect to the other 15 neurons and themselves. The output of a neuron is connected directly to the input of each synapse. The synapse output is connected to the input nodes of the next neurons through an nMOS switch. By choosing whether the switch is closed or open, one can connect arbitrarily any neuron to the others. White noise is applied through the V-I converter to each neuron. A single source of noise (noise of an on-chip resistor) distributes the noise to all neurons of an island to emulate potential local fluctuations affecting all the neurons similarly within the same neuronal island. A distinct noise generator solicits each island to emulate distinct regions with no common local potential fluctuations.

A random network topology (figure 3(C)) is configured on the 16-neuron network. The random structure is selected in each island by the random permutation function in MATLAB. Where n random synapse IDs are selected out of 256 synapses in each neuronal island. We define four islands of such 16-neuron SNN as shown in figure 3(B). Each island of neurons consists of different network topologies. In each island, 92% of the synapses are excitatory and 8% inhibitory, which emulates a reasonable average ratio typical of realistic biological networks of spiking neurons.

In figure 3(B), circles and hexagons represent neurons and synapses, respectively. The green synapses are those activated. For instance, in row number 4 (R4) of island 1 (top left), the 10th synapse is green, indicating that neuron N4 stimulates neuron N10 through that synapse. In the first island (top left), we implement a low-density connection in a random topology By 25 connections; on the contrary, in the second island (top right), we implement a higher density of 50 connections in order to demonstrate the influence of the variation of the number of connections of each island on the correlation of the spiking activities. Such difference is reflected in figure 5(A), where the correlation of island 1 is lighter than that for island 2.

We adopt the same random network topology on the third (bottom left) and fourth (bottom right) islands to observe the variation of spiking activity of neurons when we inject uncorrelated sources of noise to the same network topology. As described, all neurons in each island are connected to a single source of the noise.

3. Results

3.1. Correlation-rate of spontaneous activity of groups of neurons

The correlation coefficient matrix is calculated for three different experiments and graphically represented in figure 2. In the no-bond structure, the correlation of the synchronized bursting activity was high only for neurons belonging to the same island and were otherwise nearly zero. By connecting the islands of biological

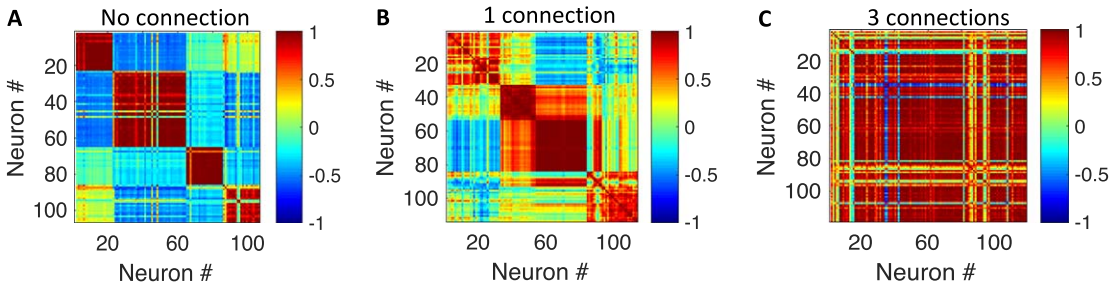

Figure 2. The Pearson correlation coefficient matrix of 4 islands of biological neurons represented in figure 1(C). The color-bar shows the amount of correlation coefficient from uncorrelated regions (blue) to highly correlated areas (dark red). In case A, the islands are not connected and the correlation is significant only for neurons within the same island. In cases B and C, the correlation progressively increases by adding 1 and 3 pathway connections respectively among the islands in a ring topology.

neurons by an individual connection, the correlation among different islands is switched. Finally, in the triple-bond structure, the correlation is high across nearly all neuron pairs.

These results confirm the findings reported in [69] and were used as reference datasets for the numerical and circuit modeling (see sections 3.2 and 3.3).

The observations indicate that the neural correlation can be controlled using micropatterned substrates by changing the number of interconnections. This is in agreement with a previous work which showed that the likelihood of an activity being transferred between two neuronal populations increased with the number of interconnecting micro tunnels in a microfluidic device [80].

The spontaneous activity in biological neuronal networks is triggered by the spontaneous release of either synaptic vesicles or ion channel stochasticity, which temporally induce fluctuation of the neuronal membrane potential. It is interesting from an engineering point of view that up to 80% of the metabolic energy consumed in the brain seems to be used in maintaining the spontaneous activity [81]. Their possible role in neural computation has been suggested to include learning [23], event directionality [24], stochastic resonance [25], management of binocular rivalry [27], and coherence [29], just to mention some examples. In the next section, we design an artificial version of this experiment to evaluate and predict some attributes of the system. Notwithstanding, a full understanding of the functional role of such an energy-consuming background activity awaits further research.

3.2. Simulation of Islands of Silicon Neurons with Internal Low-Density Connectivity

We aim to characterize the influence of spike trains generated by distinct regions and observe how the correlation among spiking activity is created thanks to the propagation of the signaling on the receiving neuron's surrounding network. The correlation propagates thanks to interneurons' equivalent, and synchronization of spiking activity is rapidly achieved when few inter-connective synapses are employed.

To investigate the variation of correlation between the spiking activities in different islands, we perform simulations by using the network represented in figure 3(B).

In the first configuration, the islands of neurons are not mutually connected. By applying uncorrelated current-mode white noise with a power of 200 $pA/\sqrt{Hz}$ to the islands for a simulation time of 240 μs, we obtain the spiking activity of the neurons represented in figure 3(D). As a result, we observe highly correlated firing activity only from neurons of the same island.

In the second simulated configuration, four islands of neurons are connected in a ring topology through interconnected synapses, such that island one is connected to island two by means of 8 one-to-one interneurons via unidirectional synapses, in the same way, the island two is connected to island 4, the 4 to the 3, and the 3 to the island 1. In such ring topology, we achieved the spiking activity of the neurons represented in figure 3(E), which shows correlation.

In order to assess the correlation quantitatively, we explore the correlation coefficient matrix. Figure 4 illustrates the correlation coefficient matrices of spiking activity of islands of silicon neurons in the mentioned simulations. In matrices, the correlation spectrum color-bar represents uncorrelated regions with blue and highly correlated regions with dark red.

When the islands are not connected (figure 4(A)), as a result of applying the same noise to all the neurons of an island, mutually connected by synapses, the self-spiking activity of the islands is highly correlated while, like in the case of biological neurons, neuron activity across different islands is not correlated.

When islands are connected (figure 4(B)) using synapses, each island's activity spreads to neighboring islands, a high correlation involves all the neurons of the network. Qualitatively, to observe a similar correlation to the biological case with only one pathway, eight one-to-one connections are needed, suggesting that either

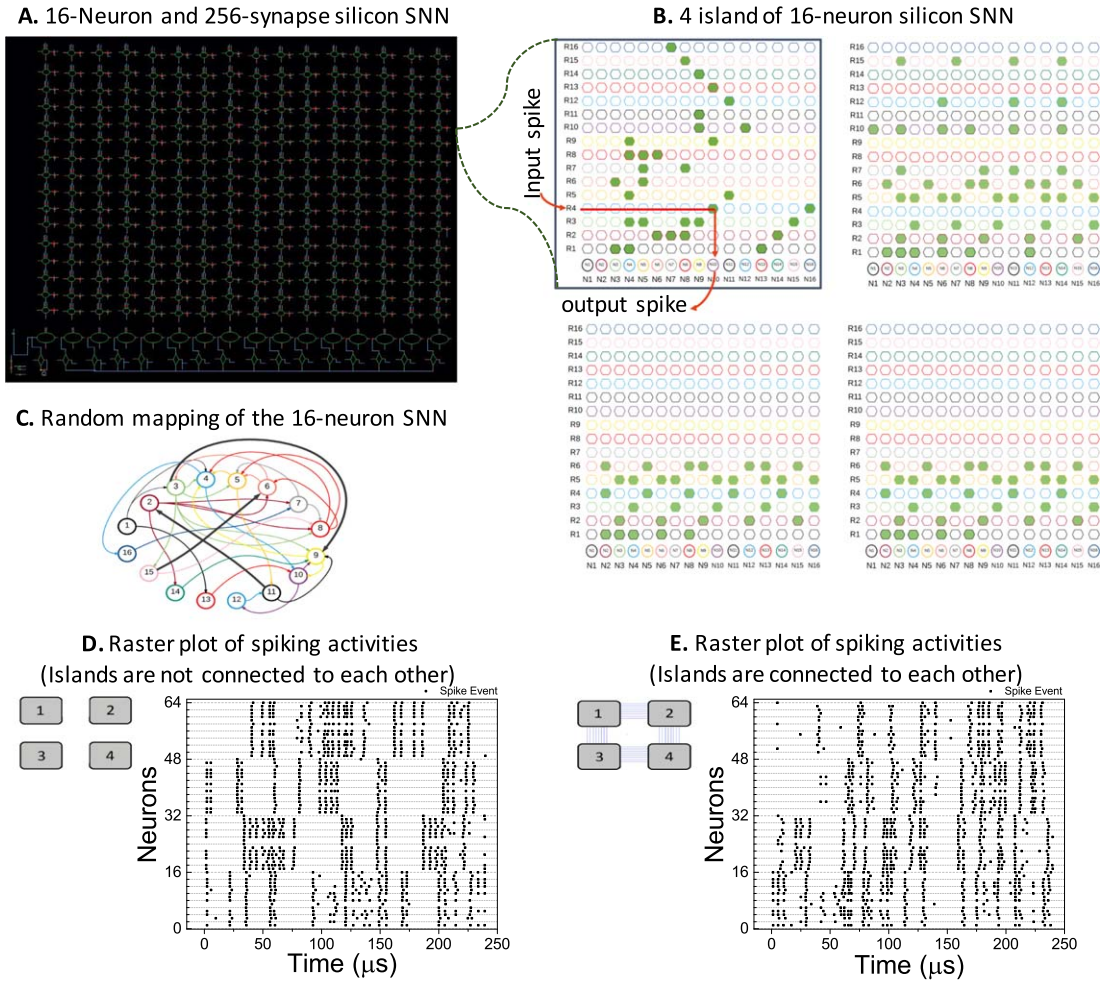

Figure 3. Injection of noise into a network of spiking neurons. (A) Network of 16 neurons (ellipses on the bottom of the diagram) and 256 synapses (circles). One V-I converter (diamond boxes, the bottom of the diagram) has been utilized for each neuron. (B) Four islands of 16 neurons employed for simulation of noise-induced activity and control of correlation by adding connections equivalent to interneurons. Neurons of the same island are connected to the same source of white noise, which is, in turn, uncorrelated to the white noise sources igniting the other islands. 8% of synapses are inhibitory. (C) A random topology realized on the 16-neuron network shown in part A. Thick black arrows represent inhibitory synapses, while other arrows are excitatory synapses. (D) Spiking activity of the neurons of the four islands network excited by white noise. The black dots show the spike event of a neuron. Neurons N1-N16 belong to the first islands, N17-N32 to the second island, N33-N48 to the third island, and N49-N64 to the fourth island. The spiking activity of neurons is correlated within the same island and uncorrelated between distinct islands. (E) Spiking activity of the neurons in case of D when the islands are connected through 8 distinct interneurons. The spiking activity of neurons of distinct islands becomes correlated.

several neurites connect the biological neuron islands or several synapses per neuron are involved. The condition of multiple synapses associated with the same neuron is developed in the next section.

3.3. Simulation of islands of neurons with multiple synapses

To achieve a high correlation between the island by employing only a few neuron connections, the micro-connectome of the artificial interneurons here consists of adding multiple synapses to the interneurons.

Figures 5(A) to (D) represents the correlation matrix of the activity of the neurons in cases of isolated islands, which refer to the connections represented in 5(E) to (H) respectively. Cases A-E provide the background of the correlation when there is no connection among neurons of distinct islands. Cases B-F represent a limiting case when one neuron excited by three synapses solicits 15 over the 16 neurons of the neighboring island (3×15). It is worth noting that even if almost all the neurons of the next island are solicited, the correlation does not saturate among distinct islands. At a microscopic level, we may interpret this due to the difficulty of affecting by an individual spiking signal the activity within the island, whose neurons are synchronously solicited by the local noise. The case C-G with three connections of kind (3×8) shows a much stronger correlation even if the number of synapses to input neurons on the next islands are cut off a half, thanks to the triple excitation connection. Such a condition provides a result that is closer to the 3N pathway connection of biological islands. The difference from the previous case can be interpreted by the combined action of more distinct input signals

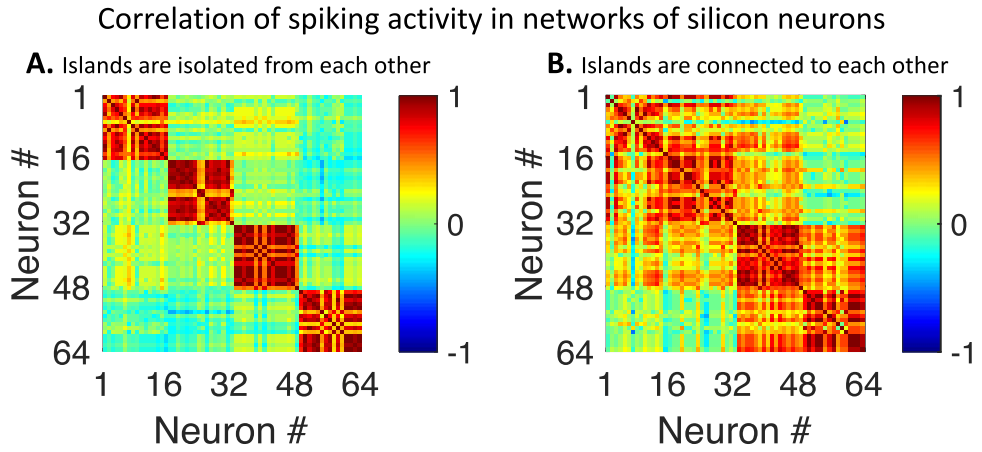

Figure 4. Pearson correlation of spiking activity of networks of artificial neurons. The color-bar shows the correlation coefficient from uncorrelated regions (blue) to highly correlated areas (dark red). A) Pearson correlation of the activity of a network of silicon neurons where islands are not mutually connected. Spiking activity is highly synchronized inside each island but almost uncorrelated among different islands. B) Correlation coefficient matrix when the island of silicon neurons (represented in (figure 3(E))) are communicating with each other by eight one-to-one interneurons in a ring topology.

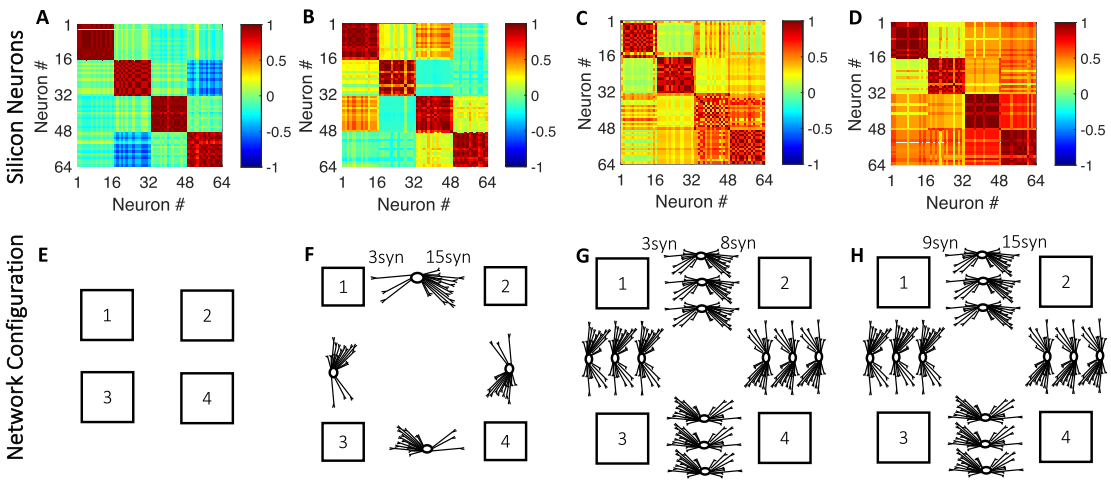

Figure 5. Pearson correlation of spiking activity of networks of artificial neurons. In all graphs, the color-bar shows the correlation coefficient from uncorrelated regions (blue) to highly correlated areas (dark red). Correlation activity in islands of (A) silicon neurons isolated from each other. (B) silicon neurons with one interneuron connection in a ring topology of kind ($1 \times 3 \times 15$). (C) Silicon neurons with three interneuron connections ($3 \times 3 \times 8$) in a ring topology, (D) silicon neurons with three connections interconnectivity ($3 \times 9 \times 15$), (E) Silicon interneuron topology without connections among islands, (F) case of one connection per pair of islands linked as a ring, of kind ($1 \times 3 \times 15$) (G) case of three connections per pair of islands linked by ($3 \times 3 \times 8$), which shows a correlation matrix similar to biological network with a triple bond. H) The limiting case of three connections of kind ($9 \times 3 \times 15$).

interfering with the synchronous activity within the island, therefore partially breaking its correlated spiking activity and therefore leaving room for the action of the other input signals. Finally, the case D-H of three (9×15) connected neurons represents again a limiting case where almost all the neurons of the next islands are fed, which exhibits even higher (but not saturated despite the connection to all the neurons of the next island) correlation. The lack of saturation is a consequence of having imposed distinct noise fluctuations on all the neurons of each island, a simplified biological system model. The biological system and the artificial CMOS system ignited by noise, as discussed above, behave very similarly. The findings suggest that in the biological islands, the spontaneous connections along the pathways by neurites of neurons in distinct islands, despite the difficulties of the process adopted from Sect. 2, are very likely and very efficient. In the spirit of indicating future refinements of the noise injection in artificial neuron system, we also observe that the assumption that a single local noise affects the sub-populations of neurons may be relaxed by reducing the influence radius of each source of noise to only first neighbors.

4. Conclusions

To conclude, we prepared and experimentally characterized a biological system comprising four populations of about 25 neurons each, attached to engineered scaffolds, and mutually connected in a ring topology by pathways where neurites can grow. Neurons adhered and grew neurites only on the permissive domains defined by the scaffolds and the pathways. The number of neurites is tuned by varying the number of available pathways to control the degree of correlation of the spiking activity among the neurons of distinct populations. Three connections per pair of populations are sufficient to spread an almost complete correlation of the whole network. Next, we designed and simulated the artificial version of such a system by an artificial network of CMOS silicon neurons operating in speed mode. The silicon system includes both excitatory and inhibitory synapses, and it is equipped with interneurons to enable communication between distinct islands, which induce spontaneous firing into higher correlation. We proposed a robust implementation of artificial silicon neurons by designing compact electronic CMOS microcircuits equipped with white and pink noise generators. We employed noise to activate the spontaneous firing activity of the neurons, and we characterized the statistics of the response of individual neurons to noise. Finally, the simulations of a ring of four noise–activated silicon islands are assessed by varying the number of interneurons and synapses. The correlation between distinct islands is more effectively increased by adding synapses to interneurons than additional independent interneurons. The results observed on the artificial neuron system suggest that the biological network is effective in the formation of synapses during its growth after the adhesion process on the micropatterned substrate.

Acknowledgments

E.P. acknowledges JSPS Fellowship, the Hokkaido University, and the Short Term Mobility Program 2016 of CNR. Part of this work was carried out under the Cooperative Research. Project Program of the Research Institute of Electrical Communication, Tohoku University. This work was supported by KAKENHI (18K19026) by Ministry of Education, Culture, Sports, Science and Technology (MEXT), Japan. The Authors thank Sho Kono, Koji Ishihara, and Soya Fujimori (Waseda University) for technical support during the fabrication. R.H. was partially supported by the Horizon-2020 ECSEL Project grant No. 783 163 (iDev40), the Austrian Research Promotion Agency (FFG), Project No. 860 424. and by Boeing, USA.

Appendix A. Design of circuits used as network elements

A.1. Fast-mode (HH) CMOS Silicon Neuron

Circuit of figure 6(a) realizes a sodium-potassium conductance-based model of spiking neurons biased in sub-threshold regime [72]. Capacitor C_{m} stands for the membrane capacitance. When a positive input current stimulates the capacitance, it starts to be charged, and consequently, the membrane potential, V_{m}, increases. When V_{m} reaches V_{Na}^{th}, transistor M1 turns on and sinks current I_{M1}. The current I_{M1} is mirrored by the transistor M4 and creates the sodium activation current, I_{Na} which builds up the up-swing of the action potential. Simultaneously, I_{M1} is also mirrored by the transistor M5 to charge the capacitor C_N, thus increasing exponentially the current I_K of the transistor M6. Therefore, V_{m} quickly drops to its resting potential. The threshold of activation of the sodium conductance is set by V_{Na}^{th}. It controls the threshold of the firing of the neuron. Pulse width of the spike is controlled by $I_{Na}^{\max}$ through $V_{Na}^{\max}$. The neuron's refractory period is set by the voltage V_R controlling the current I_R of the transistor M7. The neuron is designed such that it fires three orders of magnitude faster than the biological neurons. This has been obtained using small value capacitors ($C_m = C_N = 500fF$) with a beneficial effect on the area occupation. The size of a single CMOS neuron is $35 \times 35\ \mu\mathrm{m}^2$, six times smaller than previous implementations [82, 83].

A.2. Excitatory CMOS Silicon Synapse

Biological synapses are modeled by an exponentially decaying time-course, having different time constants for different types of synapses [85]. In order to implement a silicon synapse, we have used a current-mode low-pass filter described by a first-order differential equation of the type:

$$\tau \dot{I} = -I + I_{in}, \tag{1}$$

where I stands for the output current, τ is the constant time of the synapse and I_{in} represents the input stimulus to the synapse, [85]. The time constant is three orders of magnitude faster than that of biological synpses to be compatible with the silicon neuron. The differential-pair integrator (DPI) circuit [79] shown in figure 6(b) is designed as an excitatory synapse. Voltage-spikes from the presynaptic neurons arrive at the input-transistor, QMN_{in}, and are converted into current-inputs. By applying trans-linear principle in which, the sum of transistor

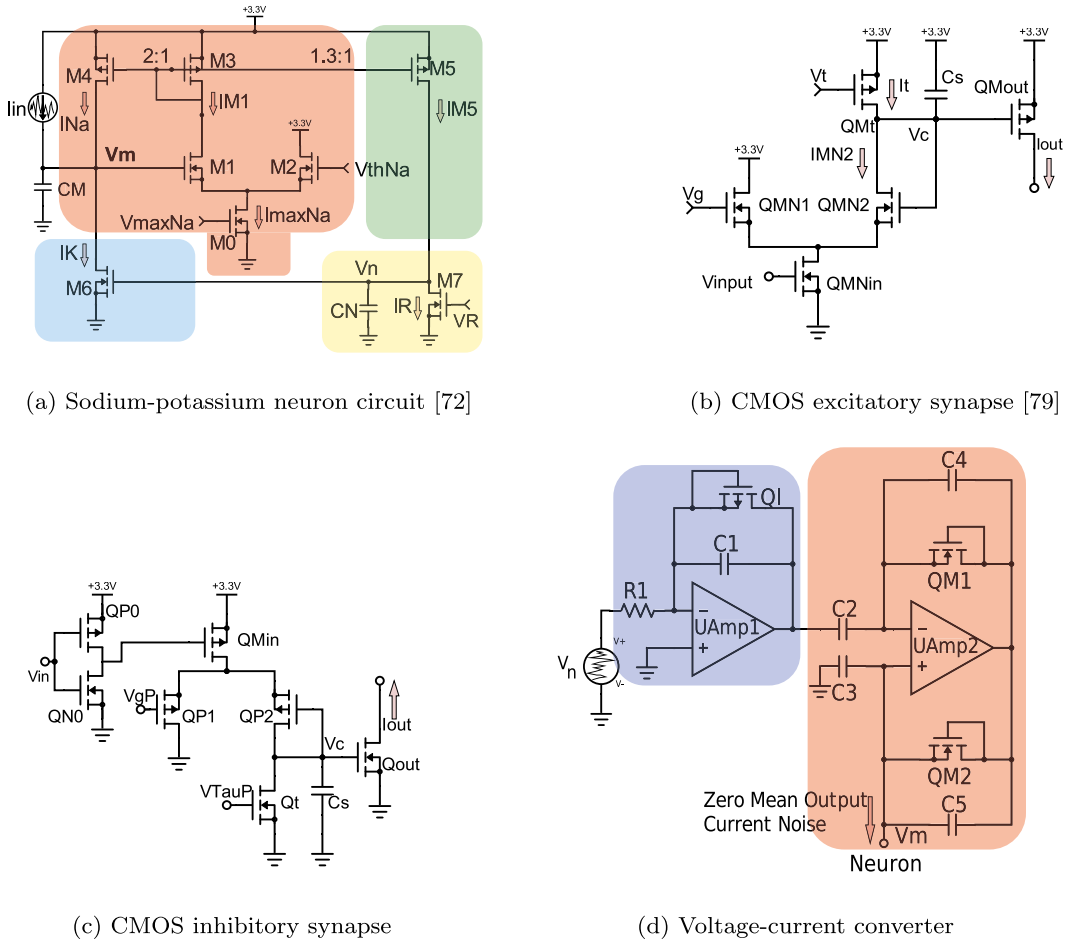

(a) Sodium-potassium neuron circuit [72]

(b) CMOS excitatory synapse [79]

(c) CMOS inhibitory synapse

(d) Voltage-current converter

Figure 6. Schematic of the network elements. (a) CMOS implementation of a fast-mode sodium-potassium neuron. The neuron circuit comprises a voltage-gated sodium conductance channel (red), a voltage-gated potassium channel (light blue), a coupling element between the sodium and potassium channels (green) and a refractory period tuner (yellow). The voltage, $V_{\rm m}$, on capacitor $C_{\rm m}$ is the membrane potential. Biasing voltages V_{Na}^{th}, $V_{Na}^{\max}$ and V_R set the threshold for firing, pulse width and refractory period of the action potential, respectively. The value of capacitors together with input current I_{in} determines the frequency of firing of the neuron. (b) CMOS implementation of an excitatory synapse using a current-mode log-domain CMOS differential-pair integrator (DPI) [79]. (c) Complementary DPI synapse circuit designed and utilized as inhibitory synapse. (d)A CMOS voltage to current (V-I) converter with a very low output dc current designed for converting the thermal noise of a resistor into a zero-mean white noise current. The V-I converter circuit consists of a modified Howland current source structure (red) [84] together with an integrator(blue). The current noise is applied as input to each neuron in order to induce stochastic behavior of spiking neurons.

voltages can be replaced by the multiplication of their currents [86], and by writing the current-voltage relationship of the capacitor C_s, the dynamics of the circuit can be presented as:

$$\tau \frac{d}{dt} I_{out} = -I_{out} + I_{in} \frac{\left(\frac{I_{out}}{I_t}\right)}{1 + \left(\frac{I_{out}}{I_t}\right)}, \tag{2}$$

where the time constant is $\tau = \frac{C_s U_T}{k I_t}$ in which C_s represents the synapse capacitor, k is the sub-threshold slope factor and U_T stands for the thermal voltage. Note that by adjusting the value of the synapse capacitor, C_s, and I_t one can control the time constant of the synapse.

A.3. Inhibitory CMOS Silicon Synapse

The inhibitory synapse consists of a complementary version of the excitatory synapse shown in figure 6(b). Figure 6(c) represents the inhibitory synapse circuit. The working principle of such a circuit is similar to that of an excitatory synapse. All nMOS transistors are replaced with pMOSs and vice versa. At the input of the inhibitory synapse, a CMOS inverter circuit consisting of the transistors indicated as QP0 and QN0 are used to invert the upcoming voltage-spikes from the presynaptic neuron. Eventually, an inhibiting current pulse I_{out} is generated at the circuit's output once the synapse gets stimulated from a presynaptic neuron.

A.4. Current Noise Generator

Many methods to implement integrated noise generators are reported in the literature based on the direct amplification of the thermal noise of a resistor [87], oscillator-sampling architectures [88], and deterministic chaos [89]. The output of such noise generators is a voltage with the desired power spectral density. To inject a current noise compatible with the silicon neuron, the two-stage voltage-to-current converter shown in figure 6(d) is designed. The output current should be in the range of hundreds of nA, at zero-mean, independent of the neuron's input voltage and with a bandwidth up to a few MHz to allow the operation of the neurons in speed-mode. To satisfy all these requirements, we have designed the bi-directional current source structure shown in the red box of figure 6(d). A Howland architecture [84] is used and specifically modified to have a very high output impedance (in the range of tens of GΩ), maintaining compatibility with standard CMOS technology. The large resistors required by the standard Howland circuit are substituted with the small value capacitors (100fF) C2-C5. To provide DC feedback to the operational amplifier UAmp2, we add the transistors QM1 and QM2 in parallel to C4 and C5, respectively. They are used as pseudo-resistors [90] to have a high resistance (hundreds of GΩ) occupying a small silicon area. In addition to a high output impedance, the pseudo-resistors implement an effective AC coupling that reduces the mean value of the injected noise to less than $1pA$ for a noise current as large as a few μA. rms The modified Howland circuit converts the input voltage into a current with a conversion factor given by the admittance of capacitor C2. Thus the output current would increase with the frequency given a white noise as input. To recover a flat frequency response from the noise source to the output current, the voltage noise source is first amplified with the integrator stage shown in blue in figure 6(d) and then converted into a current with the modified Howland circuit. An additional pseudo-resistor implemented with QI avoids the saturation of the operational amplifier UAmp1 in the integrator stage, assuring a DC feedback path. The power spectral density of the output current results $V_n/R1^2 \cdot (C2/C1)^2$, where V_n is the input voltage noise.

Such circuit is able to convert a voltage noise with a non-zero mean in a zero-mean white or pink current noise compatible with the silicon neurons above. The physical source of the noise is a resistor followed by a voltage amplifier as in [87]. White noise is obtained by amplifying the thermal noise of a non-biased resistor. By forcing a current through the resistor, a pink noise ($1/f$ noise) proportional to the current's square is generated [91], amplified and used as input of the voltage-to-current converter. The gain of the voltage amplifier is tuned to change the power of the current noise injected in the neuron. Tuning of the power has been obtained with an ideal voltage amplifier that assures a frequency response independent of the power noise to simplify the comparison of the simulation results with different noise amplitudes.

Appendix B. Correlation coefficient matrix calculation

We aim to mathematically characterize the influence of spike trains generated by the neurons of each island and observe how the correlation among spiking activity is created. For this purpose we use Pearson correlation coefficient of two random variables which is a linear measure of their dependence [92]. If each of the variables has N samples, the Pearson correlation coefficient is defined as:

$$\rho(A,\,B) = \frac{1}{N-1}\sum_{i=1}^{N}\left(\frac{A_i - \mu_A}{\sigma_A}\right)\left(\frac{B_i - \mu_B}{\sigma_B}\right), \tag{3}$$

where μ_A and σ_A are the mean and standard deviation of A, respectively, and μ_B and σ_B are the mean and standard deviation of B. Correlation coefficient can be written in terms of covariance of A and B:

$$\rho(A,\,B) = \frac{A,\,B}{\sigma_A \sigma_B} \tag{4}$$

The correlation coefficient matrix of two random variables for all pairs of variables as the following:

$$R = \begin{pmatrix} \rho(A,\,A) & \rho(A,\,B) \\ \rho(B,\,A) & \rho(B,\,B) \end{pmatrix} \tag{5}$$

A and B are directly correlated to themselves thus the diagonal entries of the matrix are 1. The matrix is symmetric such that $\rho(A, B) = \rho(B, A)$

$$R = \begin{pmatrix} 1 & \rho(A,\,B) \\ \rho(B,\,A) & 1 \end{pmatrix} \tag{6}$$

Since spiking activities of the neurons inside the 64 neuron network are random variables, we can simply build their correlation coefficient matrix (64×64) in order to find their dependence quantitatively. For calculating the correlation coefficient matrix of the spiking activity of neurons, we utilize MATLAB function

`corrcoef`(X). It returns the matrix of correlation coefficients for X, where the columns of X represent random variables and the rows represent the samples.

Appendix C. Quantification of the noise-response of a single CMOS neuron

In this section, we investigate the white and pink noise-response of a single Hodgkin-Huxley (HH) spiking neurons [71] which is designed and simulated in a 350 *nm* CMOS technology [57, 72]. A sodium-potassium conductance-based model of spiking neurons biased in the sub-threshold regime is implemented. Neurons are designed with a lower time-constant to spike three orders of magnitude faster than real neurons (more details on the implementation are provided in appendix A). Such speed-mode implementation allows faster data processing and carries as a by-product a decrease of the capacitor values used in the circuit, resulting in a reduction of its size. To model the background noise, we designed a voltage to current converter capable of delivering a zero-mean white and pink current noise to the neurons (see appendix A). In general, noise is naturally present in CMOS devices, from white and pink ($1/f$) noise [73], to telegraph noise [74], to $1/f^{1/2}$ noise [77]. The most straightforward strategy consists of amplifying such natural noise and exploiting it in the circuit by injection in the selected nodes. We now turn to the response of a single silicon neuron to the input noise to address the stochastic nature of the spiking activity, the inter-spike interval (ISI) distribution of the spiking activity, and the relationship between input current noise amplitude and the spiking rate of the neuron, respectively. Two transient 50 ms simulations of the silicon neuron are performed in Cadence and Spectre simulator, where white and pink-noise are injected into the neuron. The RMS amplitude of the current noise in both cases is equally set to 1.5 μA. Such noise value causes the neuron to generate an adequate spike rate to perform ISI and inter-train intervals (ITI) analysis. As a result, one can explore the features of the neuron's responses to different noise spectrum signals and compare how the inter-spike intervals ISI and ITI are affected. Figure 7(A) shows the power spectrum of the current noise employed for the simulations. The noise spectrum covers the operating frequency of the silicon neuron (1MHz) and starts from a frequency much lower than the typical spiking activity, shown in figure 7(C) for white and pink noise.

ISI distribution of the spiking activity of a neuron helps quantify the neuron's electrical properties such as its refractory period, mean-firing rate, and randomness of the spiking pattern, and therefore of the network [93]. Figure 7(D) describes how the number of spike events varies upon increasing the amplitude of the input noise. Normally, the silicon neuron spikes with an amplitude of 2.5V when a deterministic current stimulates it. For detecting a spike, a threshold voltage above which the counter identifies a spike is determined as follows. Figure 7(D) includes the trend of the number of detected spikes versus injected input noise for different spike detection thresholds. Counting stabilizes for the detection threshold voltage of 1 V. For a threshold of less than 1 V, random fluctuations would be considered spike events, therefore, affecting relevant information. Figure 7(E) shows the ISI histogram for the 50 ms transient simulation of the silicon neuron by injecting a zero-mean white noise to its input. The simulation is repeated for four different amplitudes of the injected input white noise ranging from 350 to 600 $pA/\sqrt{Hz}$. By increasing the amplitude of the noise, the histogram is denser and shifted to shorter time intervals. The vertical line shows the natural period of spike activity of the neuron in case of a constant input current, with amplitude equivalent to the noise RMS values injected in the simulations. A high number of spike events lay on the left side of their corresponding no–noise simulation results. Notice that the cross point of each histogram with its corresponding no–noise condition happens approximately at the same spike rate. ISI and ITI of the spiking activities of the silicon neuron between the case of white and pink noise stimuli are compared in figures 7(E) and (F). The pink noise makes a longer tail on the histogram than the white noise in agreement with other reports [94]. Furthermore, the histogram in the case of white noise is much denser than the one in pink noise. This implies that the white noise stimulus increases the excitability of a neuron within its natural refractory period at a higher rate than the pink noise stimulus. In addition to analysis on the ISI distributions, we also plot the ITI histograms to see how different noise sources affect the propagation of a train of spike events. For both white and pink noise stimuli, the distribution of spiking activity is approximately concurrent. For the simulation of the correlation among the islands discussed in section 2.2, we adopt white noise, which proves more effective to induce the neurons' excitation from the ISI point of view.

ORCID iDs

Enrico Prati https://orcid.org/0000-0001-9839-202X

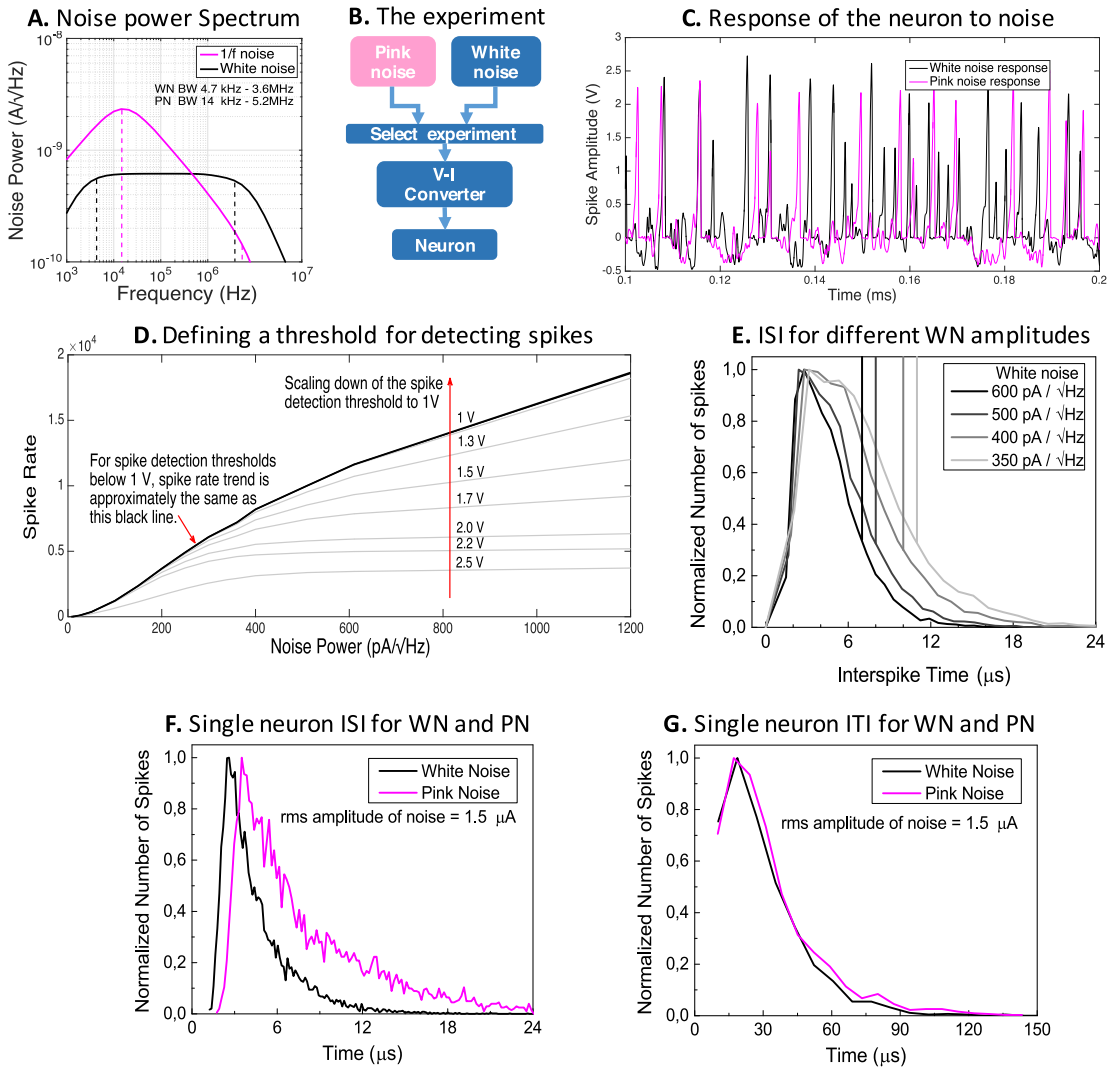

Figure 7. Injecting noise into an individual silicon neuron. (A) The power spectrum of the white and pink noise. The circuital constraints determine limitations on the noise bandwidth. (B) Flowchart of the simulation of a single neuron stimulated by noise. (C) Response of the silicon neuron to white and pink noise input current, respectively, with an RMS amplitude of 1.5 μA. (D) Determination of the threshold voltage to identify all the spikes induced by the noise injection. The counting stabilizes for a threshold voltage of 1 V. (E) Inter-spike intervals (ISI) histogram for the 50 ms transient simulation of the silicon neuron, applying a zero-mean white noise to its input. The histogram is denser by increasing the amplitude of the noise and shifted to the shorter time intervals. This is due to the reduction of the relative refractory period of a neuron due to the increase of the excitability of the neuron in the case of a stronger input stimulus. The vertical lines show our silicon neuron's response in case of a constant input current with an amplitude equivalent to the noise RMS values injected in the circuit. (F) Comparison of the ISI of the spiking activity of the neuron stimulated by white and pink noise, respectively. (G) comparison of the inter-train intervals (ITI) histogram of the spiking activities of the neuron under white and pink noise stimulation, respectively.

References

[1] Buldyrev S, Cruz L, Gomez-Isla T, Gomez-Tortosa E, Havlin S, Le R, Stanley H, Urbanc B and Hyman B 2000 Description of microcolumnar ensembles in association cortex and their disruption in Alzheimer and Lewy body dementias *Proc. Natl Acad. Sci.* **97** 5039–43

[2] Jones E G 2000 Microcolumns in the cerebral cortex *Proc. Natl Acad. Sci.* **97** 5019–21

[3] Haeusler S and Maass W 2007 A statistical analysis of information-processing properties of lamina-specific cortical microcircuit models *Cerebral cortex* **17** 149–62

[4] Haeusler S, Schuch K and Maass W 2009 Motif distribution, dynamical properties, and computational performance of two data-based cortical microcircuit templates *Journal of Physiology-Paris* **103** 73–87

[5] Rinkus G J 2010 A cortical sparse distributed coding model linking mini-and macrocolumn-scale functionality *Frontiers in neuroanatomy* **4** 2010

[6] Markram H and Perin R 2011 Innate neural assemblies for lego memory *Frontiers in neural circuits* **5** 6

[7] Potjans T C and Diesmann M 2014 The cell-type specific cortical microcircuit: relating structure and activity in a full-scale spiking network model *Cerebral Cortex* **24** 785–806

[8] Opris I and Casanova M F 2014 Prefrontal cortical minicolumn: from executive control to disrupted cognitive processing *Brain* **137** 1863–75

[9] Wang X-J and Kennedy H 2016 Brain structure and dynamics across scales: in search of rules *Curr. Opin. Neurobiol.* **37** 92–8

[10] Bellec G, Salaj D, Subramoney A, Legenstein R and Maass W 2018 Long short-term memory and learning-to-learn in networks of spiking neurons arXiv:arXiv:1803.09574
[11] Sadovsky A J and MacLean J N 2014 Mouse visual neocortex supports multiple stereotyped patterns of microcircuit activity *The Journal of Neuroscience* **34** 7769–77
[12] Ocker G K, Litwin-Kumar A and Doiron B 2015 Self-organization of microcircuits in networks of spiking neurons with plastic synapses *PLoS Comput Biol* **11** e1004458
[13] Kato S, Kaplan H S, Schrödel T, Skora S, Lindsay T H, Yemini E, Lockery S and Zimmer M 2015 Global brain dynamics embed the motor command sequence of caenorhabditis elegans *Cell* **163** 656–69
[14] Kaplan H S, Thula O S, Khoss N and Zimmer M 2020 Nested neuronal dynamics orchestrate a behavioral hierarchy across timescales *Neuron* **105** 562–76
[15] Kaplan H S and Zimmer M 2020 Brain-wide representations of ongoing behavior: a universal principle? *Curr. Opin. Neurobiol.* **64** 60–9
[16] Xie K *et al* 2016 Brain computation is organized via power-of-two-based permutation logic *Frontiers in Systems Neuroscience* **10** 95
[17] Hasani R M, Fuchs M, Beneder V and Grosu R 2017 Non-associative learning representation in the nervous system of the nematode caenorhabditis elegans arXiv:arXiv:1703.06264
[18] Hasani R M, Beneder V, Fuchs M, Lung D and Grosu R 2017 Sim-ce: An advanced simulink platform for studying the brain of caenorhabditis elegans *XXXIV International Conference on Machine Learning (ICML), Workshop on Computational Biology (WCB)*
[19] Sarma G P *et al* 2018 Openworm: overview and recent advances in integrative biological simulation of caenorhabditis elegans *Philosophical Transactions of the Royal Society B* **373** 20170382
[20] Gleeson P, Lung D, Grosu R, Hasani R and Larson S D 2018 c302: a multiscale framework for modelling the nervous system of caenorhabditis elegans *Philosophical Transactions of the Royal Society B: Biological Sciences* **373** 20170379
[21] Lechner M, Hasani R, Zimmer M, Henzinger T A and Grosu R 2019 Designing worm-inspired neural networks for interpretable robotic control *2019 International Conference on Robotics and Automation (ICRA)* (Piscataway, NJ: IEEE) 87–94
[22] Hasani R, Lechner M, Amini A, Rus D and Grosu R 2020 Liquid time-constant networks arXiv:arXiv:2006.04439
[23] Burton R M and Mpitsos G J 1992 Event-dependent control of noise enhances learning in neural networks *Neural Netw.* **5** 627–37
[24] Lukashin A V, Wilcox G L and Georgopoulos A P 1996 Modeling of directional operations in the motor cortex: a noisy network of spiking neurons is trained to generate a neural-vector trajectory *Neural Netw.* **9** 397–410
[25] Nozaki D, Mar D J, Grigg P and Collins J J 1999 Effects of colored noise on stochastic resonance in sensory neurons *Phys. Rev. Lett.* **82** 2402
[26] Natschläger T and Maass W 2005 Dynamics of information and emergent computation in generic neural microcircuit models *Neural Netw.* **18** 1301–8
[27] Brascamp J W, Van Ee R, Noest A J, Jacobs R H and van den Berg A V 2006 The time course of binocular rivalry reveals a fundamental role of noise *Journal of vision* **6** 8–8
[28] Ecker A S and Tolias A S 2014 Is there signal in the noise? *Nature* **201** 4
[29] Orlandi J G, Soriano J, Alvarez-Lacalle E, Teller S and Casademunt J 2013 Noise focusing and the emergence of coherent activity in neuronal cultures *Nat. Phys.* **9** 582–90
[30] Vuković N and Miljković Z 2015 Robust sequential learning of feedforward neural networks in the presence of heavy-tailed noise *Neural Netw.* **63** 31–47
[31] Audhkhasi K, Osoba O and Kosko B 2016 Noise-enhanced convolutional neural networks *Neural Netw.* **78** 15–23
[32] Hinton G E and Sejnowski T J 1983 Optimal perceptual inference *Pattern Recognition, Citeseer Proceedings of the IEEE conference on Computer Vision and* 448–53
[33] Ackley D H, Hinton G E and Sejnowski T J 1985 A learning algorithm for Boltzmann machines *Cogn. Sci.* **9** 147–69
[34] Lizeth G-C, Asai T and Motomura M 2012 Impact of noise on spike transmission through serially connected electrical Fitzhugh-Nagumo circuits with subthreshold and suprathreshold interconductances *Journal of Signal Processing* **16** 503–9
[35] Prati E, Giussani E, Ferrari G and Asai T 2016 Noise-assisted transmission of spikes in Maeda-Makino artificial neuron arrays *International Journal of Parallel, Emergent and Distributed Systems* **32** 1–9
[36] Prati E 2016 Atomic scale nanoelectronics for quantum neuromorphic devices: comparing different materials *Int. J. Nanotechnol.* **13** 509–23
[37] Bellec G, Scherr F, Subramoney A, Hajek E, Salaj D, Legenstein R and Maass W 2020 A solution to the learning dilemma for recurrent networks of spiking neurons *Nat. Commun.* **11** 1–15
[38] Habenschuss S, Jonke Z and Maass W 2013 Stochastic computations in cortical microcircuit models *PLoS Comput Biol* **9** e1003311
[39] Maass W 2014 Noise as a resource for computation and learning in networks of spiking neurons *Proc. IEEE* **102** 860–80
[40] Hasani R M, Wang G and Grosu R 2017 Towards deterministic and stochastic computations with the izhikevich spiking-neuron model *Neural Networks International Work-Conference on Artificial* (Berlin: Springer) 392–402
[41] Selyunin K, Hasani R M, Ratasich D, Bartocci E and Grosu R 2017 Computing with biophysical and hardware-efficient neural models *Neural Networks International Work-Conference on Artificial* (Berlin: Springer) 535–47
[42] Maass W 2015 To spike or not to spike: That is the question *Proc. IEEE* **103** 2219–24
[43] Jonke Z, Habenschuss S and Maass W 2016 Solving constraint satisfaction problems with networks of spiking neurons *Frontiers in Neuroscience* **10** 118
[44] Kappel D, Habenschuss S, Legenstein R and Maass W 2015 Network plasticity as bayesian inference *PLoS Comput Biol* **11** e1004485
[45] Mostafa H, Müller L K and Indiveri G 2015 An event-based architecture for solving constraint satisfaction problems *Nat. Commun.* **6** 8941
[46] Nir Y, Fisch L, Mukamel R, Gelbard-Sagiv H, Arieli A, Fried I and Malach R 2007 Coupling between neuronal firing rate, gamma lfp, and bold fmri is related to interneuronal correlations *Current Biology* **17** 1275–85
[47] Papadimitriou C H, Vempala S S, Mitropolsky D, Collins M and Maass W 2020 Brain computation by assemblies of neurons *Proc. Natl Acad. Sci.* **117** 14464–72
[48] Riehle A, Grün S, Diesmann M and Aertsen A 1997 Spike synchronization and rate modulation differentially involved in motor cortical function *Science* **278** 1950–3
[49] McDonnell M D and Ward L M 2011 The benefits of noise in neural systems: bridging theory and experiment *Nat. Rev. Neurosci.* **12** 415–25
[50] Kumar A, Rotter S and Aertsen A 2010 Spiking activity propagation in neuronal networks: reconciling different perspectives on neural coding *Nat. Rev. Neurosci.* **11** 615–27
[51] Kohn A, Coen-Cagli R, Kanitscheider I and Pouget A 2016 Correlations and neuronal population information *Annual review of neuroscience* **39** 237–56

[52] Hens C, Harush U, Haber S, Cohen R and Barzel B 2019 Spatiotemporal signal propagation in complex networks *Nat. Phys.* **15** 403–12
[53] Metzen M G, Hofmann V and Chacron M J 2016 Neural correlations enable invariant coding and perception of natural stimuli in weakly electric fish *eLife* **5** e12993
[54] Zylberberg J, Cafaro J, Turner M H, Shea-Brown E and Rieke F 2016 Direction-selective circuits shape noise to ensure a precise population code *Neuron* **89** 369–83
[55] Joglekar M R, Mejias J F, Yang G R and Wang X-J 2018 Inter-areal balanced amplification enhances signal propagation in a large-scale circuit model of the primate cortex *Neuron* **98** 222–34
[56] Yamamoto H, Kubota S, Chida Y, Morita M, Moriya S, Akima H, Sato S, Hirano-Iwata A, Tanii T and Niwano M 2016 Size-dependent regulation of synchronized activity in living neuronal networks *Phys. Rev.* E **94** 012407
[57] Mastella M, Toso F, Sciortino G, Prati E and Ferrari G 2020 Tunneling-based cmos floating gate synapse for low power spike timing dependent plasticity *Artificial Intelligence Circuits and Systems (AICAS), IEEE 2020 II IEEE International Conference on* 213–7
[58] Cassidy A S, Georgiou J and Andreou A G 2013 Design of silicon brains in the nano-CMOS era: Spiking neurons, learning synapses and neural architecture optimization *Neural Netw.* **45** 4–26
[59] Sharifipoor O and Ahmadi A 2012 An analog implementation of biologically plausible neurons using CCII building blocks *Neural Netw.* **36** 129–35
[60] Yasukawa S, Okuno H, Ishii K and Yagi T 2016 Real-time object tracking based on scale-invariant features employing bio-inspired hardware *Neural Netw.* **81** 29–38
[61] LeCun Y, Bengio Y and Hinton G 2015 *Deep learning, nature* **521** 436–44
[62] Prati E, Fanciulli M, Ferrari G and Sampietro M 2008 Giant random telegraph signal generated by single charge trapping in submicron n-metal-oxide-semiconductor field-effect transistors *J. Appl. Phys.* **103** 123707
[63] Kaech S and Banker G 2006 Culturing hippocampal neurons *Nat. Protoc.* **1** 2406–15
[64] Shi Y, Kirwan P and Livesey F J 2012 Directed differentiation of human pluripotent stem cells to cerebral cortex neurons and neural networks *Nat. Protoc.* **7** 1836–46
[65] Wheeler B C and Brewer G J 2010 Designing neural networks in culture *Proc. IEEE* **98** 398–406
[66] Aebersold M J, Dermutz H, Forró C, Weydert S, Thompson-Steckel G, Vörös J and Demkó L 2016 Brains on a chip: Towards engineered *Neural networks, TrAC Trends in Analytical Chemistry* **78** 60–9
[67] Yamamoto H, Matsumura R, Takaoki H, Katsurabayashi S, Hirano-Iwata A and Niwano M 2016 Unidirectional signal propagation in primary neurons micropatterned at a single-cell resolution *Appl. Phys. Lett.* **109** 043703
[68] Kono S, Yamamoto H, Kushida T, Hirano-Iwata A, Niwano M and Tanii T 2016 Live-cell, label-free identification of gabaergic and non-gabaergic neurons in primary cortical cultures using micropatterned surface *PLoS One* **11** e0160987
[69] Yamamoto H *et al* 2018 Impact of modular organization on dynamical richness in cortical networks *Science advances* **4** eaau4914
[70] Merolla P A *et al* 2014 A million spiking-neuron integrated circuit with a scalable communication network and interface *Science* **345** 668–73
[71] Hodgkin A L and Huxley A F 1952 A quantitative description of membrane current and its application to conduction and excitation in nerve *The Journal of physiology* **117** 500
[72] Sarpeshkar R, Watts L and Mead C 1992 *Refractory neuron circuits, CNS Technical Report (CNS-TR-92-08)*
[73] Nemirovsky Y, Brouk I and Jakobson C G 2001 1/f noise in CMOS transistors for analog applications *IEEE Trans. Electron Devices* **48** 921–7
[74] Prati E, Fanciulli M, Calderoni A, Ferrari G and Sampietro M 2007 Microwave irradiation effects on random telegraph signal in a mosfet *Phys. Lett.* A **370** 491–3
[75] Prati E, Fanciulli M, Calderoni A, Ferrari G and Sampietro M 2008 Effect of microwave irradiation on the emission and capture dynamics in silicon metal oxide semiconductor field effect transistors *J. Appl. Phys.* **103** 104502
[76] Prati E, Fanciulli M, Ferrari G and Sampietro M 2006 Effect of the triplet state on the random telegraph signal in si n-mosfets *Phys. Rev.* B **74** 033309
[77] Prati E, Kumagai K, Hori M and Shinada T 2016 Band transport across a chain of dopant sites in silicon over micron distances and high temperatures *Sci. Rep.* **6** 19704
[78] Bigoni S, Tagliaferri M L, Tamascelli D, Strangio S, Bez R, Organtini P, Ferrari G and Prati E 2020 Observation of single phonon-mediated quantum transport in a silicon single-electron cmos single-atom transistor by rms noise analysis *Applied PhysicsExpress* **13** 125001
[79] Chicca E, Stefanini F, Bartolozzi C and Indiveri G 2014 Neuromorphic electronic circuits for building autonomous cognitive systems *Proc. IEEE* **102** 1367–88
[80] Pan L, Alagapan S, Franca E, Leondopulos S S, DeMarse T B, Brewer G J and Wheeler B C 2015 An in vitro method to manipulate the direction and functional strength between neural populations *Frontiers in neural circuits* **9** 2015
[81] Raichle M E 2006 The brain's dark energy *Science* **314** 1249
[82] Serrano-Gotarredona R, Serrano-Gotarredona T, Acosta-Jiménez A and Linares-Barranco B 2006 A neuromorphic cortical-layer microchip for spike-based event processing vision systems *IEEE Transactions on Circuits and Systems I: Regular Papers* **53** 2548–66
[83] Indiveri G *et al* 2011 *Neuromorphic silicon neuron circuits, Frontiers in neuroscience* **5** 73
[84] A comprehensive study of the howland current pump, Texas Instruments Application Report (AN-1515 A) (2008).
[85] Destexhe A, Mainen Z F and Sejnowski T J 1998 Kinetic models of synaptic transmission *Methods in neuronal modeling* **2** 1–25
[86] Gilbert B 1996 Translinear circuits: an historical overview *Analog Integr. Circuits Signal Process.* **9** 95–118
[87] Holman W T, Connelly J A and Dowlatabadi A B 1997 An integrated analog/digital random noise source *IEEE Transactions on Circuits and Systems I: Fundamental Theory and Applications* **44** 521–8
[88] Zhou S-h, Zhang W and Wu N-J 2008 An ultra-low power cmos random number generator *Solid-State Electron.* **52** 233–8
[89] Rodriguez-Vazquez A, Delgado M, Espejo S and Huertas J 1991 Switched-capacitor broadband noise generator for cmos vlsi *Electron. Lett* **27** 1913–5
[90] Harrison R R and Charles C 2003 A low-power low-noise CMOS amplifier for neural recording applications *IEEE J. Solid-State Circuits* **38** 958–65
[91] Hooge F 1994 1/f noise sources *IEEE Trans. Electron Devices* **41** 1926–35
[92] Stuart A *et al* 1968 The advanced theory of statistics *Charles Griffin*
[93] Stein R B, Gossen E R and Jones K E 2005 Neuronal variability: noise or part of the signal? *Nat. Rev. Neurosci.* **6** 389–97
[94] Sobie C, Babul A and de Sousa R 2011 Neuron dynamics in the presence of 1/f noise *Phys. Rev.* E **83** 051912